Environ Fluid Mech (2016) 16:559–574
DOI 10.1007/s10652-015-9440-1

ORIGINAL ARTICLE

Near-boundary velocity and turbulence in depth-varying stream flows

L. C. Hopkinson[1] · C. Z. Walburn[1]

Received: 1 June 2015 / Accepted: 12 December 2015 / Published online: 22 December 2015

Abstract This research examined the temporal distribution of turbulent structure near a streambank toe through the progression of a flood wave in West Run (Morgantown, WV, USA). Three-dimensional velocities and water depths were measured through a 17-h flood event. Turbulence characteristics were examined: Reynolds stresses, turbulent kinetic energy, and turbulence intensities. On average, near-boundary velocity during the rising stage was less than the falling stage, likely due to the measurement location and local roughness. The velocity vectors shifted from towards bed before the flood wave to toward the streambank during progression of the flood wave. Turbulent kinetic energy increased with increasing water depth during the rising stage. Reynolds stress, τ_{xz}, increased with increasing water depth during the rising stage, but the majority of the stresses were negative through the storm event. Reynolds stress, τ_{xy}, was positive throughout the event and did not vary with depth. This work is among the first to evaluate turbulence during depth-varying flows in the field.

Keywords Turbulence · Unsteady flow · Open-channel flow

1 Introduction

Unsteady flows are frequent events in natural rivers as they occur during the passing of a flood wave. While unsteady, depth-varying flows are common in natural flow regimes, many studies to date evaluate turbulent structure during steady flow conditions. Therefore, more is known about the turbulent structure of flow over gravel beds during uniform, steady conditions. For example, ejections and sweeps are present [1–3], vortex

✉ L. C. Hopkinson
Leslie.Hopkinson@mail.wvu.edu

[1] Civil and Environmental Engineering, West Virginia University, PO Box 6103, Morgantown, WV 26506, USA

shedding around protruding elements of bed microtopography (i.e. pebble clusters) contributes to turbulence [2, 4–6], and the development of flow structure scales with roughness [1, 7]. Large-scale turbulent structure has been described as alternating high-speed and low-speed wedges; and, large-scale eddies scale with flow depth and initiate due to bursting in the turbulent boundary layer [8]. These previous studies show that turbulent flow structure depends on roughness and hydraulic conditions such as flow depth and velocity. While the findings have been confirmed in the field and laboratory, few studies have been completed with unsteady, depth-varying flow conditions. Additional knowledge of the instream turbulence during the passing of floods is needed to better understand river processes and sediment transport (e.g. lateral migration, fluvial erosion, and bedforms).

A better understanding of turbulence in open-channel unsteady flows is needed but is challenging to undertake [9]. Existing studies related to unsteady open-channel flow have been implemented in controlled, open-channel flume systems (e.g. [10–13]). Nezu and Nakagawa [11] and Nezu et al. [13] performed turbulence measurements over a smooth wall in a flume using a laser-Doppler anemometer. They reported greater turbulence and bulk velocity during the rising stage as compared to the falling stage of the simulated hydrograph. Song and Graf [12] evaluated mean flow and turbulence parameters of flow over a gravel bed. Measurements were completed in a flume channel during simulated hydrographs using an acoustic Doppler velocity profiler. Song and Graf [12] also reported that point velocities, turbulence intensities (horizontal and vertical), and Reynolds stresses were generally greater during the rising stage than during the falling stage of the hydrographs for a fixed water depth. Nezu et al. [13] extrapolated results to sediment transport by concluding that sediment transport would be greater during the time of rise than fall because maximum shear stress was attained during the rising stage.

These works were completed in controlled systems with smooth, symmetrical hydrographs that are not often observed in natural systems. Storm hydrographs are influenced by storm dynamics and watershed characteristics [14]. For example, steep hydrographs with high peak flows are observed when a rainstorm travels in the direction of flow [14, 15]. Spatial variability of rainfall impacts runoff timing, and temporal variability of rainfall impacts peak flowrates [14]. Therefore, a better understanding of turbulence in natural, open-channel, unsteady flows is needed.

This work evaluated turbulent structure at the streambank toe during depth-varying flow in a natural stream during the passing of a flood wave following a precipitation event. Near-boundary time-averaged velocities and turbulence statistics were evaluated. We focused on the near-bank toe location to better understand near-streambank processes. This region is of importance because erosion of the bank toe is one factor in leading to bank instability susceptible to mass failure.

2 Methods

Velocities were measured near the streambank toe through the progression of a flood wave resulting from a 1.5 cm precipitation event in October 2011. Methods are detailed in the following sections.

2.1 Study site

Data were collected in one cross section in a nearly straight section of West Run in Morgantown, WV, USA (39°40′12.3″N, 79°57′51.9″W, Fig. 1). Morgantown has an average annual precipitation of 1.05 m and is located in the Western Allegheny Plateau. The study site is located in a watershed (22 km^2) with high levels of urban development.

The channel cross section was surveyed (Leica TC600 Total Station) following the procedures recommended by Harrelson et al. [16] before and after the storm event. The cross section had an average bankfull width, bankfull depth, and slope of 8, 1.2, and 0.008 m, respectively (Fig. 2). The cross-sectional area remained within 99 % of the pre-storm area. A modified Wolman [17] pebble count was conducted before and after the storm, and the median particle size of the bed sediment decreased from 41 to 31 mm. Median grain size of the bank sediment was 0.275 mm (ASTM Standard D422-63). Grasses existed along the bank face. The vegetation was not present at the near-bank toe location where velocities were measured but interacted with the depth-varying region. Based on four random samples, average stem density was determined to be 0.33 stems/cm^2 along the bankfull bank face; stem diameters ranged from 0.1 to 0.4 cm.

2.2 Field methods

Near-bank three-dimensional velocities were measured at 7-min intervals throughout the 17-h storm event using a Sontek 16-MHz ADV Field (San Diego, CA, USA). The velocity

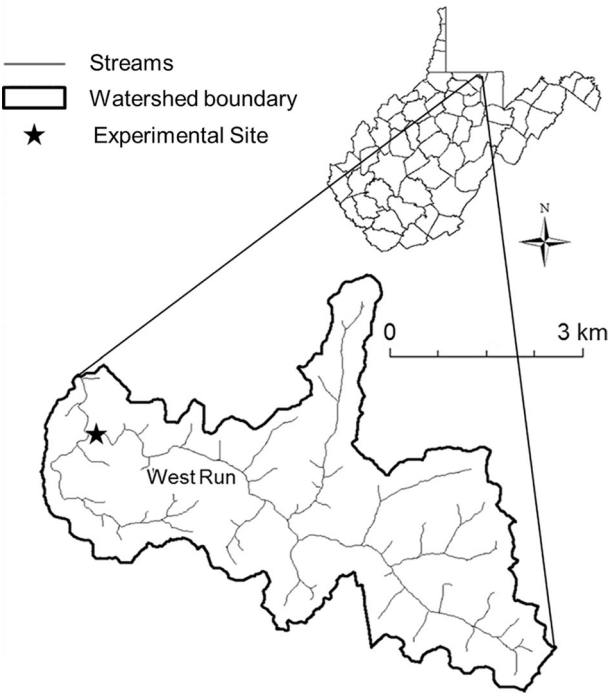

Fig. 1 West Run watershed located within West Virginia, USA. Location of experimental site identified

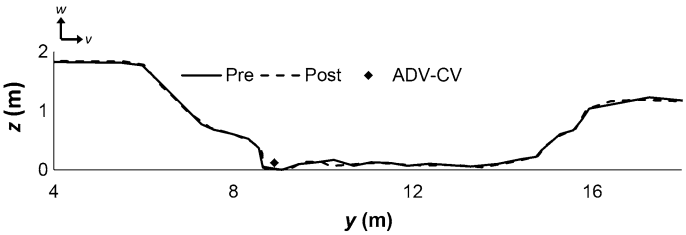

Fig. 2 Experimental cross section measured before and after the storm event (flow direction out of the page); ADV-CV represents the location of the velocity measurement control volume

measurement location was positioned near a streambank toe at a distance of 12 and 27 cm from the bed and bank, respectively (Fig. 2). These distances were as close to the boundaries as measurements could be made while both maintaining high signal quality of the velocity probe at a range of discharges and reducing the likelihood of probe to be struck by bed sediment during high flows. This location was chosen because the channel is actively widening, and the banks were a significant source of sediment. Locations of bank fluvial erosion were observed along nearly straight sections upstream of our measurement location. We intended to evaluate near-bank turbulence through the storm event to determine if any insight could be provided for the observed fluvial erosion of the cohesive streambanks.

Velocity was measured for 110 s at 25 Hz, meeting the minimum sample time suggested by Buffin-Bélanger and Roy [18]. Each velocity sample was followed by a 5 min rest period. Velocity measurements began before the storm event and continued until depths decreased to pre-storm levels. Instantaneous velocity values with an average signal correlation value <70 % or an average signal to noise ratio less than 15 were removed [19]. When 15 % of the instantaneous values were discarded from a time series, the time series was removed from further analysis [20]. A stage reading was recorded simultaneously with the velocity measurements using a strain gage pressure transducer.

2.3 Velocity and turbulence statistics

Mean turbulence variables were quantified using the three-dimensional velocity data. The velocities u, v, and w were defined as flow in the streamwise (x), lateral (y) and vertical (z) directions, respectively (where $u = \bar{u} + u'$, $\bar{u}$ = mean velocity, u' = instantaneous velocity fluctuation). Velocity vector magnitude, M, was calculated for each velocity time series ($M = \sqrt{\bar{u}^2 + \bar{v}^2 + \bar{w}^2}$).

Turbulent kinetic energy (TKE), mean kinetic energy per unit mass, was calculated:

$$\mathrm{TKE} = 0.5\left(\overline{u'^2} + \overline{v'^2} + \overline{w'^2}\right). \quad (1)$$

The overbar represents a time average. The root mean square of each velocity component was also reported (RMSu, RMSv, and RMSw), representing the turbulence intensities.

Reynolds stresses were calculated using the covariance of the streamwise and vertical velocity component (Eq. 2) and using the covariance of the streamwise and lateral velocity component (Eq. 3):

$$\tau_{xz} = -\rho\overline{u'w'}, \tag{2}$$

$$\tau_{xy} = -\rho\overline{u'v'}, \tag{3}$$

where ρ is water density.

2.4 Quadrant analysis

A quadrant analysis was completed to determine the dominance of turbulent flow events contributing to $u'w'$. Quadrant contributions were identified for each time series considering four distinct quadrants: (a) "outward" events (Q1: $u' > 0$, $w' > 0$); (b) "ejections" (Q2: $u' < 0$, $w' > 0$); (c) "inward" events (Q3: $u' < 0$, $w' < 0$); and, (d) "sweeps" (Q4: $u' > 0$, $w' < 0$) [21]. Dominant quadrant contributions for each time series were identified at two threshold values (i.e. hole size, H). An H of 0 quantified all events, and an H of 2 quantified high magnitude events [2]. Quadrant contributions to $u'v'$ were also considered.

2.5 Statistical analysis

An unequal variances t test (Welch's t test) was used to test the hypothesis that the velocity vector magnitude and turbulences statistics were equal during the rising and falling stages. The unequal variance test was used due to the unequal sample sizes. Regression analysis was completed with the velocity vector magnitude and turbulence statistics as the dependent variables to determine if there were significant relationships with flow depth. The rising stage and falling stages were analyzed separately as a different response was expected between the two stages. A significance level of $\alpha = 0.05$ was assumed for all tests. Statistical analyses were conducted using JMP Pro software (v.11.0.0, SAS Institute, Cary, NC, USA).

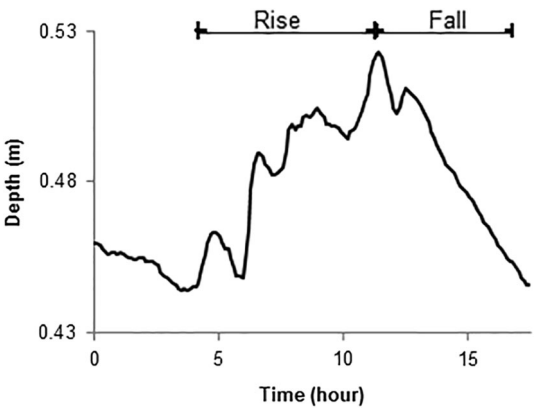

Fig. 3 Storm hydrograph with flow stages: rise and fall

3 Results

Our intent was to quantify turbulence near the streambank toe region. As such, velocities were measured throughout the storm event in close proximity to both the stream bed and one streambank (Fig. 2). The measurement location was fixed, while the water depth varied during the passing of the flood wave. The relative depth (z^*) of the measurement location varied between 0.23 and 0.27, where z^* is defined as the measurement depth (12 cm) normalized by the local flow depth (D). Therefore, all measurements were made within the inner region ($z^* < 0.3$, [22]).

Nezu et al. [13] and Song and Graf [12] both reported greater velocity and turbulence in the rising stage than in the falling stage. In these studies, velocities were measured during a simulated, symmetric hydrograph in a controlled, laboratory setting. Because our work was completed in a natural river with complex watershed contributions and precipitation patterns, the measured hydrograph did not follow a steady increase and decrease in water depth. The rising stage began when water depth increased at 4.2 h. The rising stage ended at 11.3 h when the maximum depth was observed (0.52 m). The falling stage began at 11.4 h and ended at 16.8 h when the water depth returned to the depth observed at the beginning of the rising stage (Fig. 3). The results presented in the following sections will, in part, be evaluated during these stages. Because of the complex hydrograph, there are fewer velocity measurements between depths of 0.46 and 0.48 m of the rising stage than the falling stage. Rapid water depth rise occurred during this time, 6.1–7.7 h (Fig. 3).

3.1 Time-averaged velocity and turbulent statistics

At the time before observed storm influences (time < 4.2 h), the downstream velocity component dominated the overall velocity magnitude (58–99 %). With storm influences, lateral and vertical velocity contributed up to 40 and 5 % of M, respectively (Fig. 4). Based on the unequal variance test, the mean of the M values during falling stage were greater than the rising stage (p value $= 0.0486$, Fig. 5a), and the maximum observed M over the entire flooding event occurred during the falling stage. This difference was supported by the regression analysis because the rate of increase of M with increasing flow depth was greater during the falling than rising stage (Fig. 6a; Table 1).

Velocity vectors in the lateral–vertical plane (y–z) are show in Fig. 7 because the direction and magnitude varied with water depth and time. Before the water depth began to

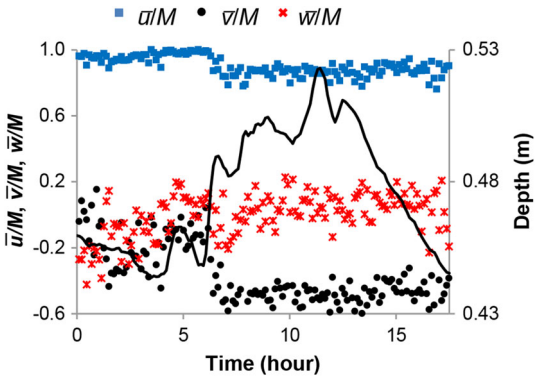

Fig. 4 Time-averaged velocity components ($\bar{u}, \bar{v}, \bar{w}$) normalized by overall velocity magnitude (M)

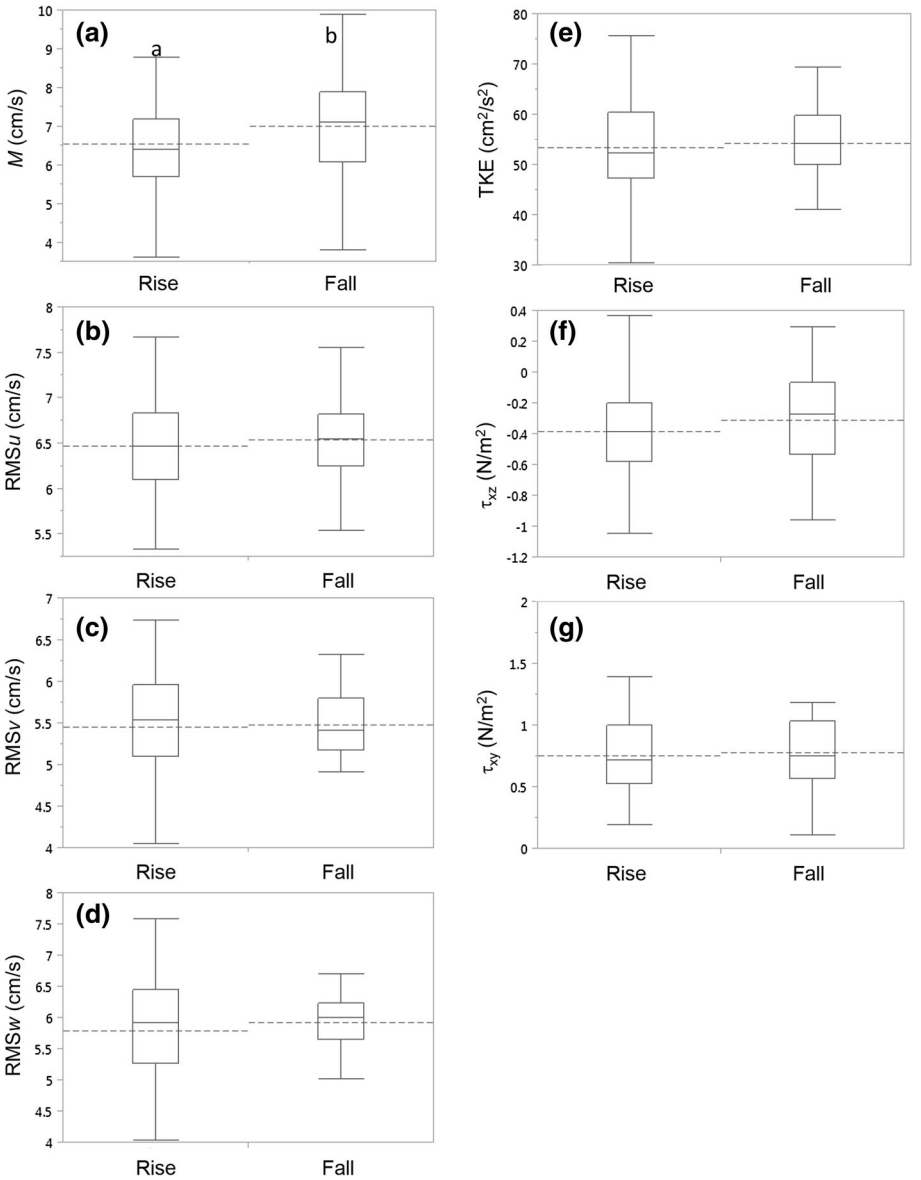

Fig. 5 **a** Velocity vector magnitude (*M*), **b–d** root mean square of the velocity components (RMS*u*, RMS*v*, RMS*w*), **e** turbulent kinetic energy (TKE), and **f**, **g** Reynolds stresses (τ_{xz}, τ_{xy}) during the rising and falling stages. Statistical significance noted with *letters*; median (–), 25–5 % (*box*), 10–90 % (*whisker*); *dashed line* represents sample mean

rise, the vertical velocity component was primarily negative (i.e. toward the bed). The vertical velocity component was primarily positive through the passing of the flood wave. The lateral velocity increased in magnitude during the storm event and was primarily directed toward the bank (Figs. 4, 7).

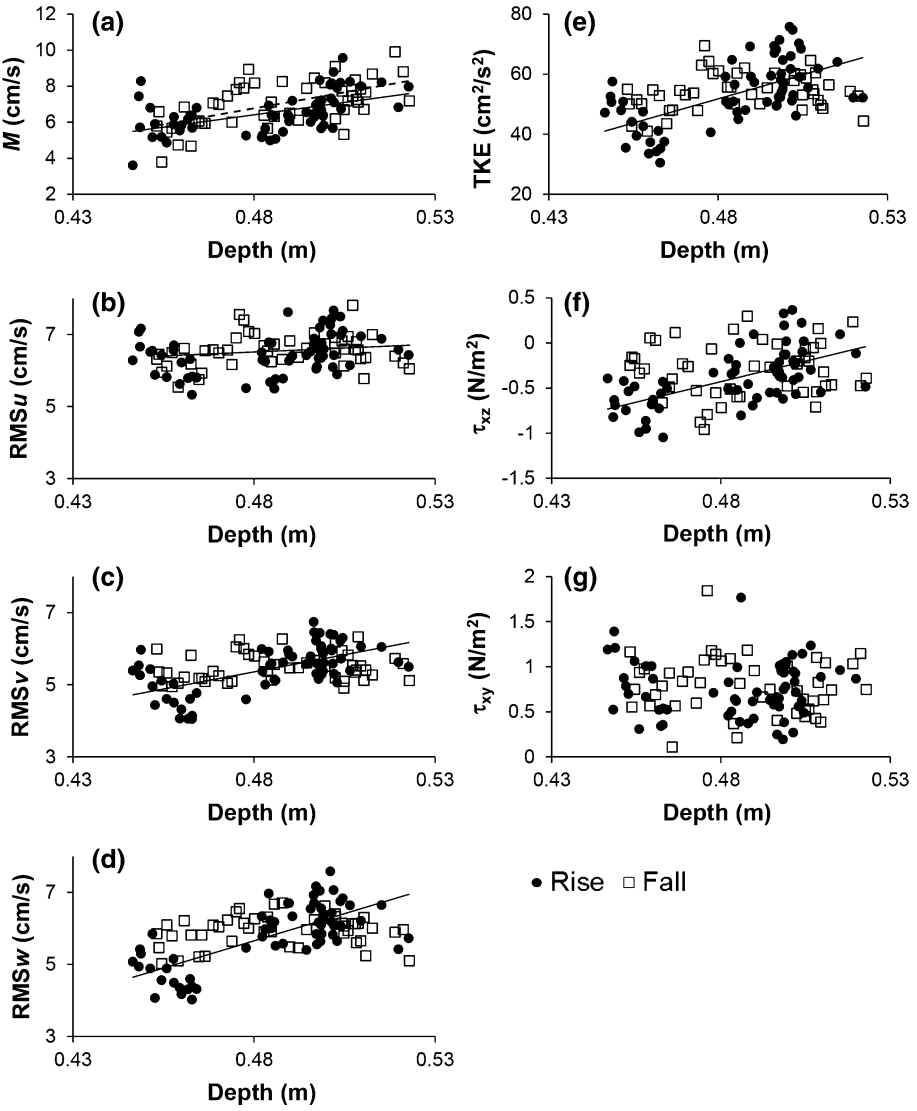

Fig. 6 **a** Velocity vector magnitude (*M*), **b–d** root mean square of the velocity components (RMS*u*, RMS*v*, RMS*w*), **e** turbulent kinetic energy (TKE), and **f**, **g** Reynolds stresses (τ_{xz}, τ_{xy}) versus water depth during time of rise and time of fall; significant linear regression shown with *solid line* for rising data and a *dashed line* for falling data

RMS*u*, RMS*v*, and RMS*w* show how velocities vary from the mean and are indicators of the violence of the turbulent fluctuations. There were no significant differences between the rising and falling stages of the streamwise (RMS*u*), lateral (RMS*v*), or vertical (RMS*w*) turbulence intensities (Fig. 5b–d). The turbulence intensities increased with increasing water depth during the rising stage. The trends were not present during the falling stage. The increasing trend with RMS*u* was statistically significant (p value = 0.013) but minor in magnitude (Fig. 6b–d; Table 1).

Table 1 Significant regression equations for velocity and turbulence statistics

Dependent variable	Intercept	Slope	p value	Adjusted R^2
Rising stage				
M (cm/s)	−6.77	27.46	<0.001	0.24
RMSu (cm/s)	2.45	8.31	0.013	0.10
RMSv (cm/s)	−3.77	19.0	<0.001	0.36
RMSw (cm/s)	−8.84	30.18	<0.001	0.50
TKE (cm/s)	−102.27	321.0	<0.001	0.37
τ_{xz} (N/m^2)	−4.80	9.09	<0.001	0.35
Falling stage				
M (cm/s)	−10.27	35.49	<0.001	0.32

All slopes are significant at $\alpha = 0.05$

No significant regression was found using τ_{xy} as the dependent variable with the data from the rising stage; no significant regressions were found using RMSu, RMSv, RMSw, TKE, τ_{xz}, and τ_{xy} as the dependent variable with the data from the falling stage ($\alpha = 0.05$)

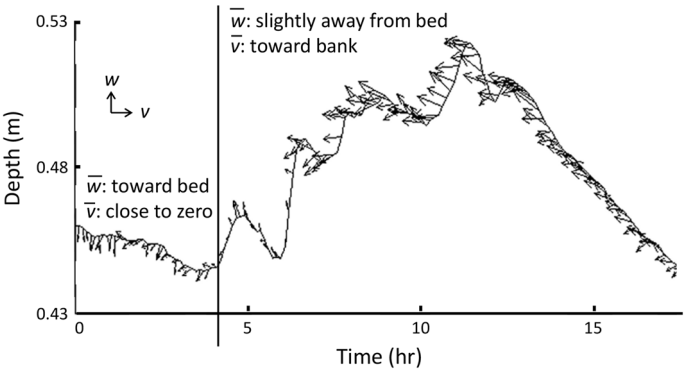

Fig. 7 Velocity vectors in lateral–vertical plane with varying water depth

Figure 8 shows each squared turbulence intensity normalized by TKE through the measured event ($\overline{u'^2}$/TKE, $\overline{v'^2}$/TKE, $\overline{w'^2}$/TKE). When the water depth was elevated due to the storm contributions, the vertical component abruptly increased, contributing up to 40 % to TKE magnitude. The lateral contribution remained constant through the measurement period, contributing up to 33 % to TKE magnitude.

During the time of most rapid water level rise (time 6.1–7.7 h), the streamwise turbulent intensity was substantially larger than the lateral and vertical contributions. Maximum TKE occurred during this time of rapid water level rise when the depth was approximately 0.5 m (Figs. 6e, 9). TKE generally increased with increasing water depth during both the rising and falling stages up to a depth of approximately 0.48 m. TKE continued to increase with increasing water depth during the rising stage, but TKE was relatively constant during the higher depths (0.48–0.52 m) of the falling stage. Therefore the only statistically significant linear trend occurred during the rising stage ($R^2 = 0.37$, Fig. 6e; Table 1).

Reynolds stress, τ_{xz}, represents the tangential on the vertical–longitudinal plane in the main flow direction, and the dominance of that component indicates momentum exchange in the streamwise direction. Before the flood wave, τ_{xz} was primarily positive. When the

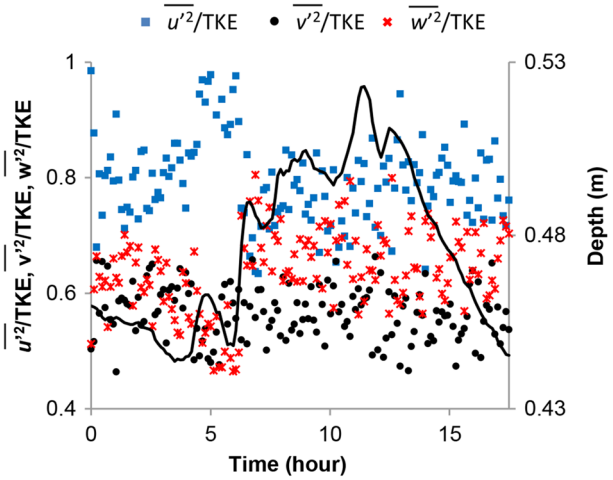

Fig. 8 *Squared* turbulent intensities normalized by TKE through the flood event shown with varying water depth

water depth began to increase, τ_{xz} was primarily negative (Fig. 9b). τ_{xz} increased with increasing water depth during the rising stage, but there was no statistical trend during the falling stage (Fig. 6f; Table 1). While not significant with depth, Fig. 9b shows a general trend of decreasing τ_{xz} with time during the falling stage.

The Reynolds stress component that represents the tangential on the lateral–longitudinal plane, τ_{xy}, was also evaluated. We considered this component because the measurements were made close to the channel bank, and wall effects were expected. All values of τ_{xy} were greater than zero. There was no trend with increasing water depth (Fig. 6g), and no differences were observed between the rising and falling stages (Figs. 5g, 9c).

3.2 Quadrant analysis

Figure 9b shows the distribution of τ_{xz} with time and compared with depth. When water depth began to rise (time = 4.2 h), τ_{xz} changed from primarily positive to primarily negative. Then, the τ_{xz} values remained negative throughout storm event. Before storm influences, the positive τ_{xz} values were a result of Q2 events ("ejections") (Fig. 10a) and high magnitude Q4 events ("sweeps") (Fig. 10b). When water depth began to rise, Q3 was the dominant quadrant ("inward" events, $H = 0$). For high magnitude events, "outward" events (Q1) dominated. The dominant quadrants were similar throughout the rising and falling stages of the hydrograph (Fig. 10).

All values of τ_{xy} were greater than zero, and there was no observed trend with water depth (Figs. 6g, 9c). For $H = 0$, Q2 events ($u' < 0$, $v' > 0$) were dominant for more than 99 % of the velocity time series. The dominant quadrant shifted to Q4 ($u' > 0$, $v' < 0$) when considering only high magnitude contributions to $u'v'$.

4 Discussion

In a laboratory study, Nezu and Nakagawa [11] reported that the maximum bulk velocity occurred over a smooth bed before the water depth reached its maximum. Song and Graf [12] also reported greater velocities in the rising stage; however, the magnitude of the difference varied by hydrograph shape and measurement location. In contrast to these

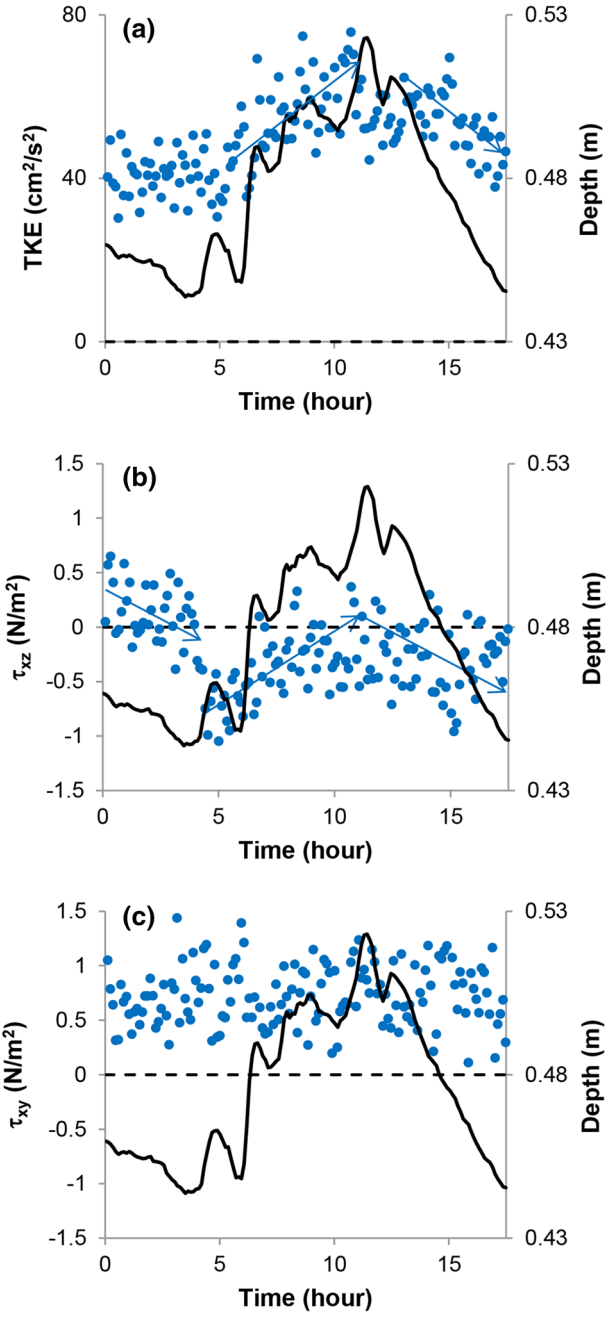

Fig. 9 Time distribution: **a** TKE, **b** τ_{xz} and **c** τ_{xy} shown with varying water depth

previous flume studies, our velocity measurements near the bank toe suggest that M was larger during the falling stage of the hydrograph than the rising stage (Fig. 5a).

As previously discussed, the measurement location was fixed near the boundary. The difference in velocity observed in flume studies [11–13] may be observed if we considered bulk velocity or velocity measured at a constant z^* through the event. Song and Graf [12]

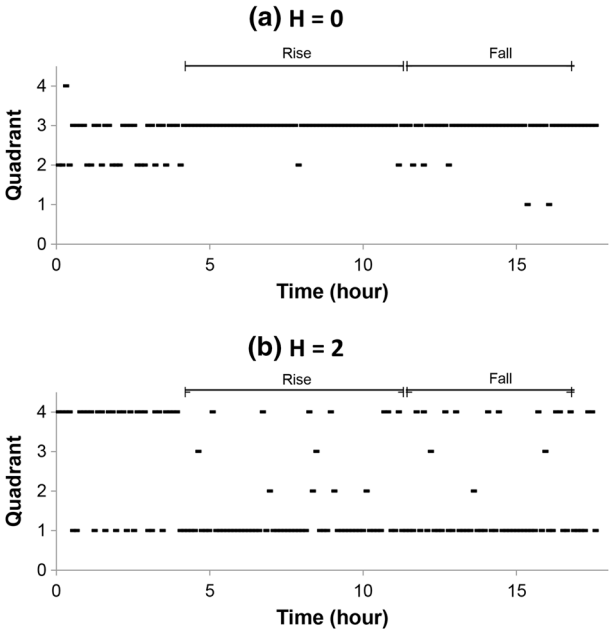

Fig. 10 Dominant quadrant contributing to $u'w'$ for hole sizes: **a** $H = 0$ and **b** $H = 2$

noted that near-bed peak velocities occurred after those near the free surface. Because we measured velocity near the boundary, the peak was likely delayed compared to the free surface.

The boundary roughness also likely contributed to the differences in velocity measurements during the rising and falling stages of the hydrograph. Clifford [23] reported few differences in velocity in locations of high relative roughness until subjected to high flowrates. Because the velocity measurements in the present study were made near the streambank toe, both bank and bed roughness influenced the time-averaged velocity. Relative roughness (D_{50}/D) of the median bed particle size (D_{50}) ranged from 0.08 to 0.09. Considering large bed particles of the 84th percentile (D_{84}), relative roughness (D_{84}/D) ranged from 0.25 to 0.29. While not in the baseflow channel, grass was located on the channel banks and interacted with the flow at the initiation of increased flow depth. Throughout the time period of depth-varying flow, the banks had varying combinations of submerged and non-submerged flexible vegetation, and the resistance of submerged vegetation increases with decreasing submergence [24]. In addition, the vegetation likely moved through three configurations as the discharge increased and decreased: erect, waving, and prone [25, 26]. Therefore, the vegetation provided varying degrees of roughness. While vegetation was not monitored through the event, it was prone for a short time following the flood event. It might be that the vegetation remained prone during the falling stages, providing less resistance for the falling stage, contributing to the greater mean velocity values.

A change in overall velocity vector direction was observed during the measured time period (Fig. 7). Before storm influences (time < 4.2 h), the time-averaged velocity vector is primarily directed toward the bed. The direction changes to away from the bed through the progression of the flood wave. During the storm influences, lateral velocity increases in magnitude. The lateral velocity was close to zero before a time of 4.2 h. After the time of

4.2 h, the lateral velocity increased in magnitude and was primarily directed toward the bank (Figs. 4, 7). In gravel-bed rivers at low flow, bed features (e.g. pools, riffles) influence the net direction of flow, and the direction may change at high flows [23]. French and Clifford [27] also observed a change in direction of the vertical velocity component when analyzing velocity and turbulence through the flood and ebb phase of a tidal creek. Mean velocity in the vertical direction was directed away from the bed during the flood phase and toward the bed during the ebb phase. The measurement position in the present study was located in a nearly straight section of the stream to minimize secondary flow effects, but the change in direction of the lateral velocity vector suggests that there is a counter-clockwise secondary flow cell near the study bank at flood flows. Similar flow structure has been documented by Papanicolaou [28] in a study of streambank erosion.

A substantial amount of scatter was observed in the velocity measurements, likely due in part to the short-time over which the measurements were averaged; the standard error of the three velocity components as defined by Buffin-Bélanger and Roy [18] were on the order of 10^1 cm/s. The fluctuating nature of the hydrograph also contributed to scatter. The stream did not experience a smooth increase and decrease in water depth as simulated in laboratory channels (i.e. [12, 13]).

Song and Graf [12] reported greater turbulence in the rising stage because streamwise and vertical turbulence intensities were greater during the rising stage at a fixed water depth. The difference was more evident in the inner region near the boundary. Our results showed that RMSu, RMSv, and RMSw increased with increasing depth during the rising limb. Maximum RMSv and RMSw measured during the progression of the flood wave occurred during the rising limb before the peak depth was reached. Similar trends were observed with the TKE data and suggest high turbulence during the rising limb. There are, however, a large amount of scatter in the results as well as no statistical differences in mean TKE between the rising and falling stages, so further studies are needed.

TKE values in the inner region are influenced by local bed roughness [22] as boundary layers in flows with high relative roughness are dominated by eddies [29]. For example, Tan and Curran [22] reported that TKE in the inner region increased locally due to bed roughness on the order of 50 cm^2/s^2. This result was determined from a flume study over a grave bed with no bedforms, and relative roughness was approximately 0.06. Because measurements in the present study were made in the inner region ($z^* < 0.3$, [22]), TKE was likely influenced by the bed roughness as relative roughness based on the median particle size was greater than 0.06 for the entire flow event ($D_{50}/D = 0.08$–0.09, $D_{84}/D = 0.25$–0.29). It should be noted that median particle size after the flood event was 10 mm less than pre-flood levels. The reduced bed roughness likely influenced the distribution of TKE as well as the other turbulence statistics during the flood event.

TKE was likely influenced by the bank vegetation roughness as well. Czamomski et al. [30] reported elevated turbulence intensities near the bank toe in the presence of dense vegetation. Hopkinson and Wynn [31] also observed increased near bank-toe TKE in the presence of simulated shrub vegetation as compared to a bank with only grain roughness. The same study found that the folding of bank grass dampened turbulence near the bank toe. If the vegetation was erect during the at least a portion of the rising limb and remained prone during the falling stage, less bank roughness existed during the falling stage. The greater roughness may have contributed to the increased TKE with depth during the rising stage.

Song and Graf [12] and Nezu and Nakagawa [11] reported that Reynolds stresses (τ_{xz}) were greater in the rising stage than the falling stage. The peak τ_{xz} observed in our study was observed during the rising limb; however, the majority of the stresses were negative

through the storm event, scatter was substantial, and there was no statistical difference in mean values. Before the water depth increased, τ_{xz} was primarily positive as a result of high magnitude Q4 events. During the time of depth-varying flow, few ejection or burst events were observed. Due to the measurement location, influence of the bank has to be considered. Along a streambank with simulated vegetation, Hopkinson and Wynn [31] reported that τ_{xy} was often greater in magnitude than τ_{xz}. For that reason, τ_{xy} was also considered in this study. While τ_{xy} remained positive throughout the entire observation period, no differences among rising and falling stages were observed, and τ_{xy} did not vary with water depth.

The measurement location was selected so that we could potentially provide information for entrainment of the streambank sediment. Sediment transport was not monitored through flood event, but survey results indicate that 4 mm of bank erosion occurred. Dey et al. [32] reported that sweeps are the mechanism for the initiation of sediment entrainment near the bed. In the same study, ejections were present at the top of the shear layer at the entrainment threshold. Our results show a similar distribution of sweep events during the rising and falling stages of the hydrograph (Fig. 10). Considering $H = 2$, 18 % of the rising measurements and 23 % of the falling measurements were dominated by Q2 or Q4 events. The small number of ejections and sweeps support the limited erosion that was observed.

To the authors' knowledge, no study exists that monitors streambank erosion rates through a flood event with depth-varying flow. However, bedload transport has been reported to be greater on the rising limb than the falling limb for high stress events [33]. In the same study, Kuhnle [33] also reported that bedload transport was greater during the falling stage than the rising state for a low stress event. The greater number of sweeps during the falling stage of the present study suggests that erosion rates were potentially greater during the falling stage, but further studies are needed to confirm this result.

This study was limited to a single measurement location through the rising and falling stage of a flood hydrograph. Because of the rapid nature of the depth increase during the rising stage, fewer velocity measurements were recorded between mean water depth 0.46 and 0.48 m on the rising limb as compared to the falling limb. Results may vary with different storms, as the hydrograph will vary with storm dynamics and watershed characteristics [14, 15]. The results at this site may vary as the channel geometry evolves and near bank turbulence may change with bank angle [30]; however, this work is the first step in evaluating unsteady flow in situ and shows that more work is needed in complex, natural, unsteady open-channel flows.

5 Conclusions

This study characterized the temporal variability of flow parameters near the streambank toe through the progression of a flood wave. This region is of importance because erosion of the bank toe is one factor in leading to bank instability susceptible to mass failure. This work was among the first to evaluate near-boundary flow characteristics with depth-varying flow conditions in the field. Major conclusions include:

- On average, near-boundary velocity during the rising stage was less than the falling stage, likely due to the measurement location and local roughness. Velocity increased slightly with increasing depth during both the rising and falling stages.

- The velocity vectors shifted from toward the bed before the flood wave to towards the bank during the flood wave.
- M, RMSu, RMSv, RMSw, TKE, and τ_{xz} increased with increasing water depth during the rising stage; the increase in RMSu was minor. M increased with increasing depth during the falling stage, and τ_{xy} was independent of depth.
- TKE increased with increasing water depth during the rising stage. Peak turbulent kinetic energy was observed during the rising limb before reaching the flow-depth peak. TKE was generally constant during the higher depths of the falling stage, and the variation between the rising and falling stage were minor. Bank vegetation and bed roughness likely contribution to the time distribution of TKE.
- The majority of τ_{xz} values were negative through the storm event, but τ_{xz} was affected by water level as τ_{xz} increased with increasing depth. Component τ_{xy} was positive throughout the event and did not vary with depth.

These conclusions are only valid to the near-streambank toe region evaluated in this study. Additional studies are needed to quantify the reach and cross-section turbulence during depth varying flows in natural systems.

Acknowledgments The authors would like to thank Will Ravenscroft and Karen Buzby.

References

1. Buffin-Bélanger T, Roy AG (1998) Effects of a pebble cluster on the turbulent structures of a depth-limited flow in a gravel-bed river. Geomorphology 25:249–267. doi:10.1016/S0169-555X(98)00062-2
2. Lacey JWJ, Roy AG (2008) Fine-scale characterization of the turbulent shear layer of an instream pebble cluster. J Hydraul Eng 134(7):925–936. doi:10.1061/(ASCE)0733-9429(2008)134:7(925)
3. Nezu I, Nakagawa H (1993) Turbulence in open-channel flows. Balkema, Brookfield
4. Lacey JWJ, Roy AG (2008) The spatial characterization of turbulence around large roughness elements in a gravel-bed river. Geomorphology 102:542–553. doi:10.1016/j.geomorph.2008.05.045
5. Lacey RWJ, Roy AG (2007) A comparative study of the turbulent flow field with and without a pebble cluster in a gravel bed river. Water Resour Res 43:W05502. doi:10.1029/2006WR005027
6. Robert A, Roy AG, De Serres B (1996) Turbulence at a roughness transition in a depth limited flow over a gravel bed. Geomorphol 16:175–187. doi:10.1016/0169-555X(95)00143-S
7. Hardy RJ, Best JL, Lane SN, Carboneau PE (2009) Coherent flow structures in a depth-limited flow over a gravel surface: the role of near-bed turbulence and influence of Reynolds number. J Geophys Res 114:F01003. doi:10.1029/2007JF000970
8. Hardy RJ, Best JL, Lane SN, Carbonneau PE (2010) Coherent flow structures in a depth-limited flow over a gravel surface: the influence of surface roughness. J Geophys Res 115:F03006. doi:10.1029/2009JF001416
9. Nezu I (2005) Open-channel flow turbulence and its research prospect in the 21st century. J Hydraul Eng 131(4):229–246. doi:10.1061/(ASCE)0733-9429(2005)131:4(229)
10. Tu H, Graf WH (1992) Velocity distribution in unsteady open-channel flow over gravel beds. J Hydrosci Hydraul Eng 10(1):11–25
11. Nezu I, Nakagawa H (1995) Turbulence measurements in unsteady free-surface flows. Flow Meas Instrum 6(1):49–59. doi:10.1016/0955-5986(95)93458-7
12. Song T, Graf WH (1996) Velocity and turbulence distribution in unsteady open-channel flows. J Hydraul Eng 122(3):141–154. doi:10.1061/(ASCE)0733-9429(1996)122:3(141)
13. Nezu I, Kadota A, Nakagawa H (1997) Turbulent structure in unsteady-depth varying open-channel flows. J Hydraul Eng 123(9):752–763. doi:10.1061/(ASCE)0733-9429(1997)123:9(752)
14. Singh VP (1997) Effect of spatial and temporal variability in rainfall and watershed characteristics on stream flow hydrograph. Hydrol Process 11:1649–1669. doi:10.1002/(SICI)1099-1085(19971015)11:12<1649:AID-HYP495>3.0.CO;2-1
15. Singh VP (2002) Effect of duration and direction of storm movement on infiltrating planar flow with full areal coverage. Hydrol Process 16(7):1479–1511. doi:10.1002/hyp.358

16. Harrelson CC, Rawlins CL, Potyondy JP (1994) Stream channel reference sites: an illustrated guide to field technique. Rep. no. RM-245, US Department of Agriculture, Forest Service, Rocky Mountain Forest and Range Experiment Station, Fort Collins, CO
17. Wolman MG (1954) A method of sampling coarse river-bed material. Trans AGU 35(6):951–956
18. Buffin-Bélanger T, Roy AG (2005) 1 Min in the life of a river: selecting the optimal record length for the measurement of turbulence in fluvial boundary layers. Geomorphology 68(1):77–94. doi:10.1016/j.geomorph.2004.09.032
19. Wahl TTL (2000) Analyzing ADV data using WinADV. 2000 joint conference on water resources engineering and water resources planning and management, American Society of Civil Engineers, Reston, Virginia
20. Lane SN, Biron PM, Bradbrook KF, Butler JB, Chandler JH, Crowell MD, McLelland SJ, Richards KS, Roy AG (1998) Three-dimensional measurement of river channel flow processes using acoustic Doppler velocimetry. Earth Surf Proc Land 23:1247–1267. doi:10.1002/(SICI)1096-9837(199812)23:13<1247:AID-ESP930>3.0.CO;2-D
21. Lu SS, Wilmarth WW (1973) Measurements of the structure of the Reynolds stress in a turbulent boundary layer. J Fluid Mech 60:481–511
22. Tan L, Curran JC (2012) Comparison of turbulent flows over clusters of varying density. J Hydraul Eng 138(12):1031–1044. doi:10.1061/(ASCE)HY.1943-7900.0000635
23. Clifford NJ, French JR (1993) Monitoring and modelling turbulent flow: historical and contemporary perspectives. In: Clifford J, French JR, Hardy J (eds) Turbulence: perspectives on flow and sediment transport. Wiley and Sons, West Sussex, pp 1–34
24. Wilson CAME (2007) Flow resistance models for flexible submerged vegetation. Hydrology 342(3–4):213–222. doi:10.1016/j.jhydrol.2007.04.022
25. Kouwen N, Unny TE, Hill HM (1969) Flow retardance in vegetated channels. J Irrig Drain Eng 95(2):329–344
26. Gourlay MR (1970) Discussion of 'Flow retardance in vegetated channels' by N Kouwen, TE Unny, HM Hill. J Irrig Drain Eng 96(3):351–357
27. French JR, Clifford NJ (1992) Characteristics of event-structure of near-bed turbulence in a macrotidal saltmarsh channel. Estuar Coast Shelf Sci 34:49–69. doi:10.1016/S0272-7714(05)80126-X
28. Papanicolaou AN, Elhakeem M, Hilldale R (2007) Secondary current effects on cohesive river bank erosion. Water Resour Res 43:W12418. doi:10.1029/2006WR005763
29. Kickbride A (1993) Observations of the influence of bed roughness on turbulence structure in depth limited flows over gravel beds. In: Clifford J, French JR, Hardy J (eds) Turbulence: perspectives on flow and sediment transport. Wiley, West Sussex, pp 185–196
30. Czarnomski NM, Tullos DD, Thomas RE, Simon A (2012) Effects of vegetation canopy density and bank angle on near-bank patterns of turbulence and Reynolds stresses. J Hydraul Eng 138(11):974–978. doi:10.1061/(ASCE)HY.1943-7900.0000628
31. Hopkinson L, Wynn T (2009) Vegetation impacts on near bank flow. Ecohydrology 2(4):404–418. doi:10.1002/eco.87
32. Dey S, Sarkar S, Solari L (2011) Near-bed turbulence characteristics at the entrainment threshold of sediment beds. J Hydraul Eng 137(9):945–958. doi:10.1061/(ASCE)HY.1943-7900.0000696
33. Kuhnle RA (1991) Bed load transport during rising and falling stages on two small streams. Earth Surf Proc Land 17:191–197